J. Fluid Mech. (2003), *vol.* 496, *pp.* 193–211.
DOI: 10.1017/S0022112003006323 Printed in the United Kingdom

Feedback control of oscillatory thermocapillary convection in a half-zone liquid bridge

By J. SHIOMI[1], M. KUDO[2], I. UENO[2], H. KAWAMURA[2] AND G. AMBERG[1]

[1]Department of Mechanics, Royal Institute of Technology, S-100 44 Stockholm, Sweden
shiomi@mech.kth.se

[2]Department of Mechanical Engineering, Tokyo University of Science, Chiba, 278-8510, Japan

(Received 17 October 2002 and in revised form 20 May 2003)

Active feedback control was applied to suppress oscillations in thermocapillary convection in a half-zone liquid bridge. The experiment is on a unit-aspect-ratio liquid bridge where the most unstable azimuthal mode has wavenumber 2 when control is absent. Active control was realized by locally modifying the surface temperature using the local temperature measured at different locations fed back through a simple control law. The performance of the control process was quantified by analysing local temperature signals, and the flow structure was simultaneously identified by flow visualization. With optimal placement of sensors and heaters, proportional control can raise the critical Marangoni number by more than 40%. The amplitude of the oscillation can be suppressed to less than 30% of the initial value for a wide range of Marangoni number, up to 90% of the critical value. The proportional control was tested for a period-doubling state and it stabilized the oscillation to a periodic state. Weakly nonlinear control was applied by adding a cubic term to the control law to improve the performance of the control and alter the bifurcation characteristics.

1. Introduction

Oscillatory thermocapillary convection, often blamed for the periodic variations in composition (striations) in the production of single crystals using the floating-zone method (Chang & Wilcox 1976), has been studied intensively in recent decades. In the floating-zone method, by slowly pulling a raw material through a ring heater, the small zone near the heater is melted and re-solidified as a single crystal. This containerless processing has advantages in increasing the purity of the crystal. To further increase purity, space processing has been proposed to avoid the influence of thermal convection. However, in micro-gravity conditions, oscillatory thermocapillary convection becomes significant and causes detrimental striations in the chemical composition of the finished crystal. Since the first experimental observation of the three-dimensional time-dependent state in thermocapillary convection by Schwabe & Scharmann (1979) and Chun & Wuest (1979), this problem has been a prime candidate for space-based projects. In addition, this is a rich fundamental physical problem with nonlinear dynamics which can lead the flow to chaotic states.

Many studies have been done on a simplified model, the half-zone model, which essentially models half of the floating zone. In a half-zone, a liquid drop is held between two coaxial rods maintained at different temperatures to impose an axial temperature gradient on the free surface. Preisser, Schwabe & Scharmann (1983)

found experimentally that the most unstable azimuthal wavenumber and frequency are determined by the aspect ratio of the liquid bridge. This was followed by the work of Velten, Schwabe & Scharmann (1991) where the onset of instability was experimentally measured at different high Prandtl numbers (Pr). The stability characteristics were studied using linear stability theory by Neitzel *et al.* (1993) and Kuhlmann & Rath (1993). Levenstam & Amberg (1995) carried out a numerical simulation and determined that the mechanism of the onset of the oscillatory flow for a low-Pr liquid is a purely hydrodynamic instability very similar to the instability of a vortex ring. Wanschura *et al.* (1995) examined the dependence of the onset of the instability on Pr by a linear stability analysis and drew similar conclusions. For high-Pr liquids, the instability was attributed to heat transport coupled with the Marangoni effect. In the intermediate regime ($Pr = 0.07$–0.84), Levenstam, Amberg & Winkler (2001) carried out a numerical simulation and linear stability analysis and showed that the thermocapillary forces counteract the hydrodynamical instability, and thus the axisymmetric base state is much more stable than at high or low Pr. In connection with bifurcation theory, Leypoldt, Kuhlmann & Rath (2000) have described a supercritical Hopf bifurcation by means of numerical simulation. Further increase in the temperature gradient will result in the transition to a chaotic state Ueno, Tanaka & Kawamura (2003). Recently, some interesting flow patterns have been observed in the transitional regime by Schwabe, Hintz & Frank (1996) and Kawamura, Ueno & Ishikawa (2002). On seeding the flow with particles, three-dimensional structures were revealed by particles accumulating along a single closed orbit.

One of the first works to utilize feedback control to stabilize thermal convection was by Wang, Singer & Bau (1992) who applied proportional control in a thermal convection loop, and managed to suppress the chaotic behaviour. Later, Yuen & Bau (1996) succeeded in changing a subcritical Hopf bifurcation to a supercritical bifurcation using cubic control. An attractive feature of this problem is that the system can be described well by a set of model equations which are essentially the celebrated Lorenz's equations. Based on these model equations, theoretical and numerical analyses were carried out together with experiments.

Using similar methodology, these works were followed by a series of works on Rayleigh–Bénard convection. For two-dimensional Rayleigh–Bénard convection, Tang & Bau (1993) theoretically demonstrated the possibility of delaying the onset of convection by almost one order of magnitude. This was followed by the experimental work of Howle (1997) where feedback control caused significant suppression of two-dimensional convection in a slender box. The control method was also tested for three-dimensional convection by Tang & Bau (1998), but the stabilization obtained fell far short of the theoretical prediction for two-dimensional convection.

Recently, a few theoretical works have been reported on feedback control of the transition from a no-motion state to time-independent motion in Marangoni–Bénard convection. Linear control was applied to delay the onset of the instability by Bau (1999). The delay of transition was confirmed by means of linear stability analysis. Or *et al.* (1999) demonstrated the possibility of controlling the long-wavelength mode by a weakly nonlinear control law. Nonlinear flow properties could be altered to eliminate the subcritical nature of the bifurcation. A similar analysis was applied to the finite-wavelength mode by Or & Kelly (2001), taking the buoyancy effect into account.

With this better understanding of the phenomena, some results have been reported on the control of oscillatory thermocapillary convection in various geometries. An

attempt to stabilize the thermocapillary wave instability in an experiment on a plane fluid layer was made by Benz *et al.* (1998). The temperature signal and phase information sensed by thermocouples near the cold end of the layer was fed forward to control a laser which heated the downstream fluid surface along a line. For an annular configuration, Shiomi, Amberg & Alfredsson (2001) and Shiomi & Amberg (2002) applied active feedback control based on a simple cancellation scheme. Using two sensor/actuator pairs, a significant attenuation of oscillation was observed in a range of Marangoni number (Ma), with the best performance in the weakly nonlinear regime.

For a half-zone model, Petrov *et al.* (1996, 1998) attempted to stabilize the oscillation by applying a nonlinear control algorithm using local temperature measurements close to the free surface and modifying the temperature at different local locations with Peltier devices. The control scheme is based on an idea of Ott, Grebogi & Yorke (1990). They constructed a look-up table based on the system's response to a sequence of random perturbations. A linear control law using appropriate data sets from the look-up table was computed. The control law was updated at every time step to adapt the control law to the nonlinear system. Using one sensor/actuator pair, successful control was observed at the sensor location for $Ma \sim 17750$. However, infrared visualization revealed the presence of standing waves with nodes at the feedback element and the sensor. This was resolved by adding a second sensor/actuator pair which enables the control to damp out waves propagating both clockwise and counterclockwise, thus standing waves. The performance of the control was reported for only one value of $Ma \sim 15000$, where the critical value was $Ma \sim 14000$. They stated that the oscillation could not be suppressed when Ma exceeds the critical value by more than 8.5%, mostly due to the weak response of the fluid flow to the Peltier devices, which cannot be cooled more than a few degrees during the application of the control pulse.

In the present report, we intend to control oscillatory thermocapillary convection in a half-zone through an active feedback control scheme. The control is based on a simple linear feedback control law with sensors and actuators strategically positioned based on knowledge of the dominant azimuthal mode which is determined by the geometry of the system. In contrast with the scheme of Petrov *et al.* (1996, 1998), the current method allows us to tackle the problem without constructing reference data beforehand. It was shown by Shiomi *et al.* (2001) and Shiomi & Amberg (2002) in the annular configuration that the method can stabilize the flow in a range of Maragoni number without any cooling devices.

At this stage, we can only consider a high-Pr system where heat transport plays an important role. Nevertheless, this is an attractive case for general flow control, since it is a slow phenomenon with a limited number of modes active in the global instability, and the flow can be stabilized by measuring and modifying the surface temperature, which is usually easily accessible. Furthermore, the closed geometry makes feedback control possible.

2. Experimental apparatus

The geometry of the half-zone model is shown in figure 1. The height and diameter of the bridge are $H = 2.5\,\text{mm}$ and $R = 2.5\,\text{mm}$. The diameter of the bridge was kept small enough for the thermocapillary convection to dominate the buoyancy-driven convection. T_h and T_c denote the hot and cold wall temperatures. The Marangoni number is defined as $Ma = \gamma \Delta T H/\alpha\mu$, where γ and ΔT are the absolute value of the surface tension coefficient and $T_h - T_c$, and μ and α are the viscosity and

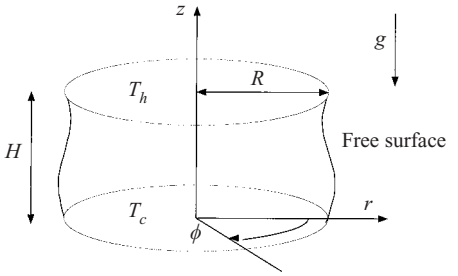

FIGURE 1. Half-zone model.

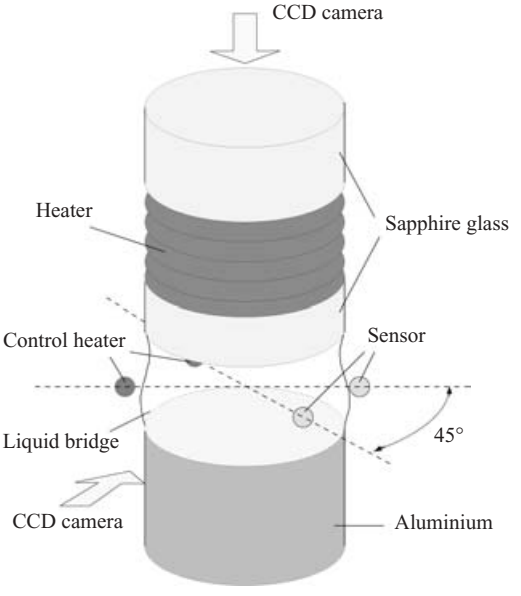

FIGURE 2. Experimental setup.

the thermal diffusivity at $(T_h + T_c)/2$. The parameter ϵ measuring the increase from the critical value of Ma is defined as $\epsilon = (Ma - Ma_{cr})/Ma_{cr}$, where Ma_{cr} is Ma at criticality. All measurements and actuations were done on the line $(r, z) = (R, H/2)$; thus hereafter among the spatial parameters only the ϕ-position will be denoted. The dimensionless temperature $\theta(\phi, t) = (T(\phi, t) - \overline{T}(\phi))/\Delta T$ is used throughout the analysis, where $\overline{T(\phi)}$ is the time average of $T(\phi, t)$.

The experiment, as described in previous reports (Kawamura *et al.* 2002; Ueno *et al.* 2003), was set up as in figure 2. An axial temperature gradient was imposed by heating the top rod with a wire heater tied around it. The bottom rod made of aluminium is connected to a heat sink to play the role of the cold wall. The top rod was made of sapphire to enable us to observe the flow field through the top end of the bridge. The sidewall of the bottom rod was coated with a fluoride paint to inhibit the liquid from wetting the side. The liquid is 5 cSt silicone oil which gives $Pr = 68$ at 25 °C. The aspect ratio Ar, defined as the ratio of the radius to height of the bridge, H/R, was 1 throughout the experiment. The ambient temperature was the room temperature.

For flow visualization, the liquid bridge was seeded with polystyrene particles with diameter 17 μm and specific gravity 1.07. Two CCD cameras were set on the top and side of the liquid bridge to capture top and side views of the structure of the convection. The whole bridge was illuminated with two continuous light sources. The view from the top was mainly used to examine the flow structure, and the one from the side was used to observe the free-surface shape. The free surface is curved as sketched in figure 2 where the volume of the liquid is approximately equal to the volume of the cylinder, $\pi R^2 H$. To carry out quantitative analysis on control performance, it is important to prevent the surface shape from changing due to evaporation, since this may affect the stability properties (Hu *et al.* 1994). Efforts were made to keep the liquid volume constant by adding liquid between measurements when needed.

Two sensor/heater pairs could be placed in different azimuthal locations. The sensors and heaters utilize the technique described in Shiomi *et al.* (2001). Calibrated cold wires were used as sensors. They have a U shape, where the curved bottom is made of a platinum wire with diameter of 2.5 μm. The distance between the two supporting prongs was 0.2 mm. Sensors were placed through the surface so that the tips of the sensors were approximately 100 μm deep. The principle is that a constant current passes through the platinum wire and detects the resistance, which is proportional to the temperature. The amount of current is limited so that the heating power of the sensor does not exceed 1 μW. Since the wire is very thin, it can be palced through the free surface without causing appreciable deformation. The control heater is made in the same manner as the sensor, but of 10% rhodium–platinum in order to enhance the resistivity. The heater is placed about 300 μm above the surface. The power output from the heaters is obtained by measuring current and voltage over the heater.

A typical experiment was carried out as follows. First, the bridge was filled with Silicone oil mixed with polystyrene particles using a syringe until the desired surface shape and bridge volume were achieved. Then T_h was increased to a few degrees below the critical value to drive a steady two-dimensional convection. A waiting period of at least 15 min was allowed in order to reach a thermal equilibrium. On raising T_h, the onset of the oscillation was observed by flow visualization, and the critical value of ΔT was recorded. Typical values of T_h, T_c and ΔT at criticality were 52 °C, 20 °C and 32 °C, respectively, for ambient temperature of about 20 °C.

When T_h was changed between measurements, care was taken that the heating ramp never exceeded 0.1 K s^{-1}, the value confirmed in advance to have little influence on Ma_{cr}. Setting ΔT to a designated value, the volume ratio was checked and, if necessary, small drops of the liquid were carefully added to the bridge with a syringe. Whenever the drops were added during the experiment, we waited for a period of at least 15 min. The probes were then installed, and the measurements were started after confirming steady oscillation by the temperature signals and flow visualization.

3. Flow without control

3.1. *Flow visualization*

Top-view flow visualization allows us to observe the mode structure in the (r, ϕ)-plane. Since the whole bridge was illuminated with continuous lighting, the views captured illustrated the fields integrated in the z-direction. After the onset of the oscillation, a polygonal particle-free area appears at the centre of the plane. As shown by Ueno *et al.* (2003) where a flow visualization was carried out for a wide range of Ar, the number of lines of symmetry in the visualized image indicates certain polygonal modal

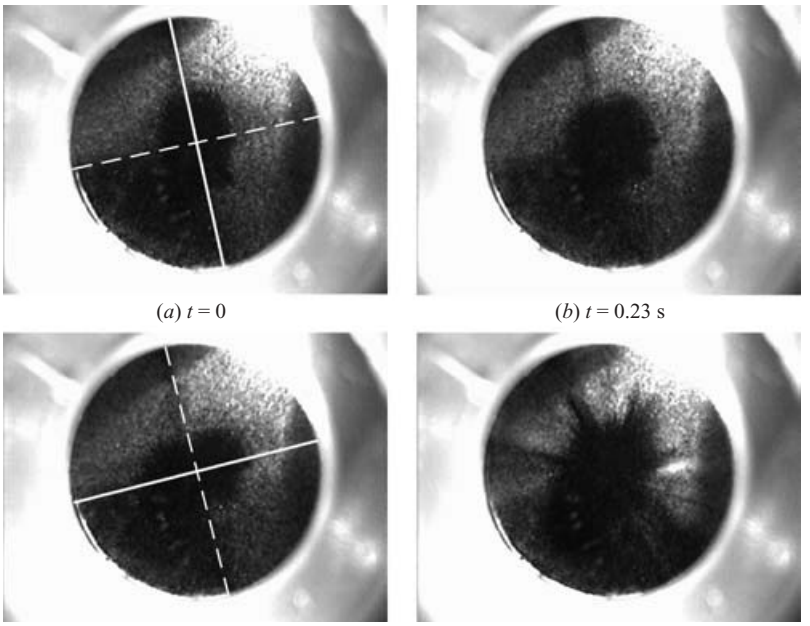

FIGURE 3. Flow visualization of a mode-2 standing wave. (*a–c*) Without control. (*d*) Time-independent state achieved by proportional control. $\epsilon = 0.18$.

flow structures. The polygonal particle-free area indicates the radial deformation of the vortical structure from the axisymmetric state. In the present setting of $Ar = 1$, the particle-free area appears to be an ellipse. Here, the number of lines of symmetry is 2; thus the oscillation has azimuthal wavenumber of 2 (mode-2).

In the regime close to criticality, the oscillation is standing. A mode-2 standing oscillation is shown by the sequence of pictures in figure 3(*a–c*). The solid and dashed lines represent the lines of symmetry. Starting from state (*a*), where the ellipse is fully elongated along the solid line, the ellipse gradually becomes circular and reaches the axisymmetric state (*b*). Then the particle-free area begins to stretch along the line normal to the initial direction of elongation until it reaches the fully elongated state (*c*). The process continues in the reverse manner as $(c) \rightarrow (b) \rightarrow (a)$. One period of oscillation has a duration of about 0.91 s. Lighting is from the bottom left direction in the pictures. Fewer particles are observed in the lower left quarter of the section because of the uneven initial distribution of the particles. When the standing wave is formed, the particles cannot cross the node lines, visualized as a dark line in the radial direction where the azimuthal velocity is zero.

On increasing ϵ ($\geqslant 0.32$, based on $Ma_{cr} = 31000$ as discussed in § 3.2), the ellipse was shown to rotate in the azimuthal direction, which indicates that the wave is travelling. In figure 4, the flow visualization of a model 2 travelling wave is shown as the sequence $(a) \rightarrow (b) \rightarrow (c)$ which corresponds to half a period of the oscillation. The solid lines represent the lines of symmetry. The direction of rotation was unpredictable, which supports the symmetry of the experimental apparatus. On further increase in ϵ, the ellipse narrows down to almost a line. At this stage, the dynamics is strongly nonlinear and the oscillation has a highly three-dimensional structure. Further information on the various flow patterns with increasing ϵ is available in Ueno *et al.* (2003).

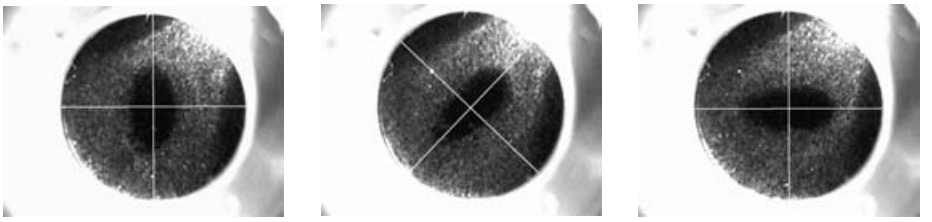

(*a*) $t = 0$ (*b*) $t = 0.23$ s (*c*) $t = 0.46$ s

FIGURE 4. Flow visualization of the mode-2 travelling wave without control for $\epsilon = 0.41$.

3.2. *Temperature measurements*

From temperature signals at two different azimuthal positions, clockwise and counterclockwise propagating waves can be identified. Since the oscillation is the result of the superimposition of two waves rotating in opposite directions, the mode n oscillation based on the fundamental frequency, $\hat{\theta}_n$, can be written as

$$\hat{\theta}_n(\phi, t) = A_{n,1}(t)\sin(n\phi - 2\pi f_n t + \eta_{n,1}) + A_{n,2}(t)\sin(n\phi + 2\pi f_n t + \eta_{n,2}), \qquad (3.1)$$

where $A_{n,1}$ and $A_{n,2}$, are the amplitudes, and $\eta_{n,1}$ and $\eta_{n,2}$ are the phases of the clockwise and counterclockwise propagating waves of mode (azimuthal wavenumber) n, respectively, and f_n denotes the critical frequency of the nth mode. Using the experimentally accessible values,

$$\hat{\theta}_n(\phi_1, t), \qquad \hat{\theta}_n(\phi_2, t), \qquad \frac{\partial \hat{\theta}_n(\phi_1, t)}{\partial t}, \qquad \frac{\partial \hat{\theta}_n(\phi_2, t)}{\partial t}, \qquad f_n, \qquad n, \qquad (3.2)$$

we can compute

$$A_{n,1}(t), \qquad A_{n,2}(t), \qquad \eta_{n,1}, \qquad \eta_{n,2}. \qquad (3.3)$$

The mode number n was obtained from flow visualization, and $\hat{\theta}_n$ was computed by applying a band-pass filter to the frequency components around the base frequency of the nth mode. The critical frequency of mode n, f_n, was detected from the peaks of the power spectra. This way, for multiple modes, we can identify each mode component and analyse its spatial structure, unless their frequency bands overlap. In the present work, $A_{n,1}(t)$ and $A_{n,2}(t)$ are always computed for periodic oscillations where they are time independent, hence the notation of time dependence for these variables is omitted hereafter.

Now we can obtain quantitative measurements on the transition from a standing wave to a travelling wave. In figure 5, the amplitudes of the clockwise and counterclockwise waves are plotted for a range of ϵ. It can be seen that up to $\epsilon = 0.32$, $A_{2,1}$ and $A_{2,2}$ show similar values, which indicates that the oscillation has a standing structure. Above this limit, $A_{2,1}$ becomes dominant which means that the structure has become a travelling one.

The data for $A_2 = (A_{2,1}^2 + A_{2,2}^2)^{1/2}$ show good agreement with a supercritical Hopf bifurcation in the weakly nonlinear regime (Iooss & Joseph 1989). For a supercritical Hopf bifurcation, the amplitudes of the oscillation should grow proportionally to the square root of ϵ. Here, the bifurcation curve (solid line) was fitted to the data, confirming the weakly nonlinear regime where the bifurcation theory should be applicable. The plots falls beneath the bifurcation curve as the nonlinearity becomes stronger, as also observed in the numerical simulation by Leypoldt *et al.* (2000). Note that this is not a case where the growth of the amplitude is restricted by becoming

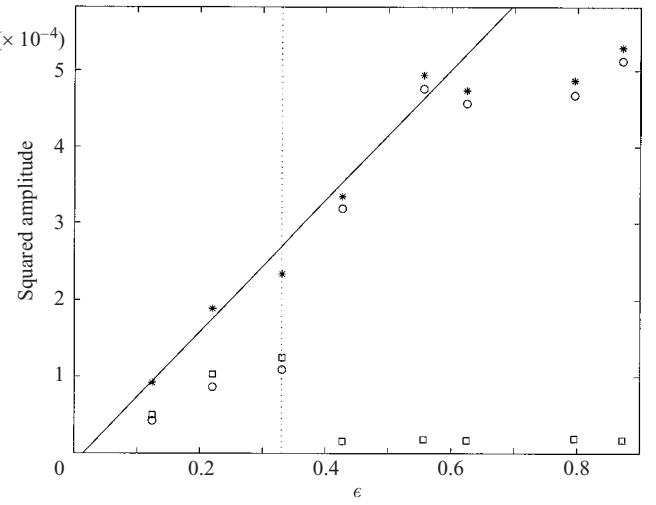

FIGURE 5. Circles: the squared amplitude of the clockwise rotating wave, $A_{2,1}^2$. Squares: the squared amplitude of the counterclockwise rotating wave, $A_{2,2}^2$. Stars: $A_2^2 = A_{2,1}^2 + A_{2,2}^2$. Solid line: the supercritical Hopf bifurcation curve fit to selected data. Ma_{cr} was determined by flow visualization. The dotted line marks the change in the flow pattern from standing to travelling waves observed by flow visualization.

comparable to ΔT, since the amplitude of a typical oscillation is about 2% of ΔT. Ma_{cr} ($\sim$31000) was determined by careful observation of flow visualization, and then confirmed to be similar to the value obtained by interpolating the bifurcation curve down to $A_2 = 0$.

3.3. *Frequency*

As numerically shown by Leypoldt *et al.* (2000), the nonlinear interaction of the modes modifies the oscillation frequencies. Since the extent of the modification should depend on the energy distribution of the two waves with opposite directions of rotation, the frequency evolves differently depending on whether the oscillation is standing or travelling. They showed that the critical frequency increases proportionally to ϵ, with different slopes depending on whether the wave is standing or travelling. The evolution of the critical frequency of a standing wave was checked up to high ϵ by generating the standing wave and extracting the frequency before the perturbation grows large enough to become a travelling wave.

Some of these features could be confirmed experimentally as shown in figure 6, where the change in the flow structure accompanies a change in the slope of the f_2 curve. The values of f_2 without control are plotted with pluses. Based on the findings of Leypoldt *et al.* (2000), we identified two kinds of frequency evolutions, f_2^{SW} (dotted line) and f_2^{TW} (dashed line), corresponding to a standing wave and a travelling wave, respectively. Up to $\epsilon = 0.32$, below which standing waves can be observed, f_2 is close to f_2^{SW}. The frequency decreases as the oscillation structure changes from standing to travelling. When the wave becomes purely travelling, f_2 is close to f_2^{TW}. Qualitatively, the results are in a good agreement with those of Leypoldt *et al.* (2000), though more data points would be required for a more accurate determination of the slopes, which now do not intersect at $\epsilon = 0$ as they should.

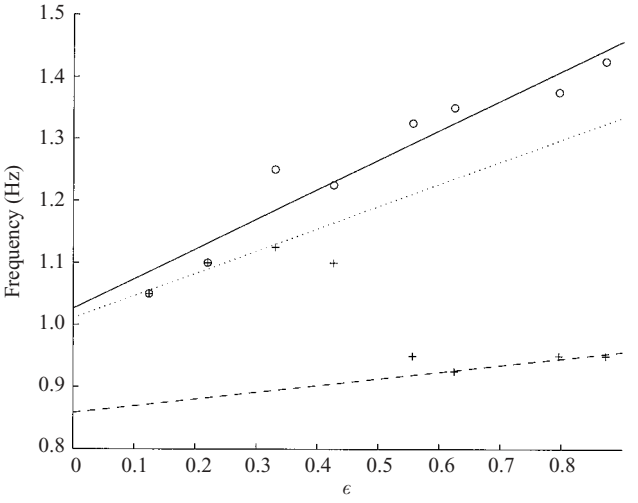

FIGURE 6. The critical frequencies f_2 of mode-2 oscillation without (+) and with (○) control ($\mathrm{d}\phi = \pi/2$).

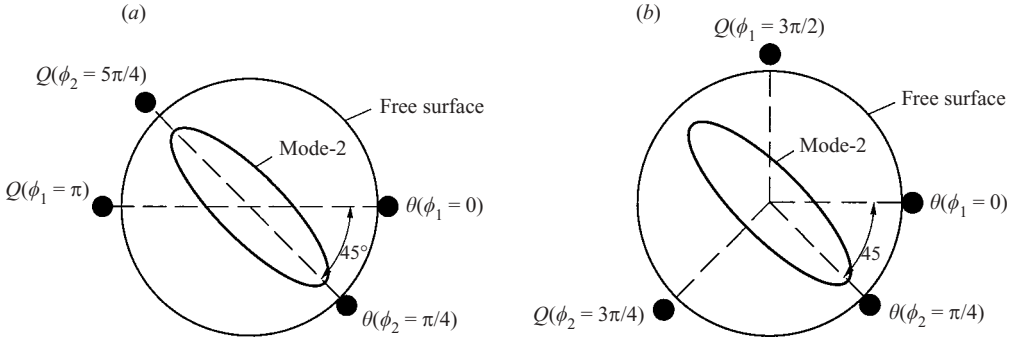

FIGURE 7. Sketch of different sensor/heater configuration. (*a*) $\mathrm{d}\phi = \pi$, (*b*) $\mathrm{d}\phi = \pi/2$.

4. Proportional control, $\mathrm{d}\phi = \pi$

4.1. *Linear control law*

With unit aspect ratio, the mode-2 oscillation dominates the flow when control is absent. This means that, at fixed radial and axial positions, $\theta(\phi)$ and $\theta(\phi + \pi)$ will be in phase. A simple cancellation scheme can be constructed if we introduce point heat sources as

$$Q(\phi_i + \mathrm{d}\phi) = -G_1\theta(\phi_i), \tag{4.1}$$

where ϕ_i is the ith azimuthal sensor location and $\mathrm{d}\phi$ is the distance between sensors and paired heaters. Q and $G_1(\geqslant 0)$ are the heater power output and proportional control gain. First we consider $\mathrm{d}\phi = \pi$. Since applying only one sensor/heater pair could result in a standing wave with nodes at the sensor/heater positions (Petrov *et al.* 1998), two sensor/heater pairs were positioned $\pi/4$ apart ($\phi_1 = 0$ and $\phi_2 = \pi/4$) as shown in figure 7(*a*). For the mode-2 oscillation, $\pi/4$ is one quarter of a wavelength. This means that we position the second sensor/heater pair at locations where the wave might have had an anti-node if we had applied only one sensor/heater pair.

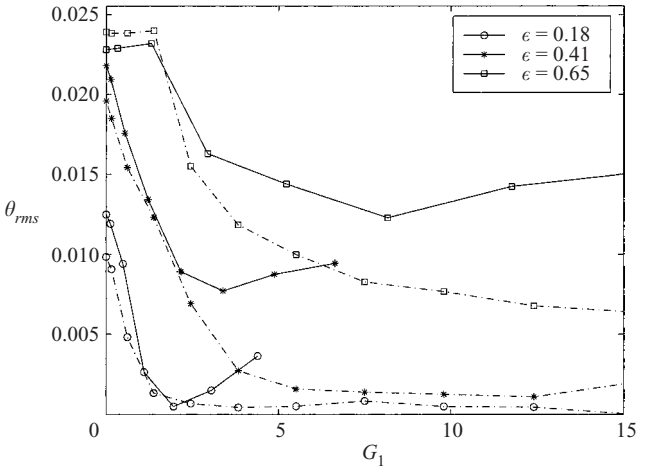

FIGURE 8. $\theta_{rms} = (\overline{\theta(\phi_1)^2} + \overline{\theta(\phi_2)^2})^{1/2}$ for various values of G_1. Solid lines: $\mathrm{d}\phi = \pi$, dashed lines: $\mathrm{d}\phi = \pi/2$, for $\epsilon = 0.12, 0.42$ and 0.62.

This configuration of probes is equivalent to the one shown in Shiomi & Amberg (2002) to achieve the best performance among cases tested with different distances between the sensors. Since the actuators used in the present experiment limit our action to heating only, the actual output from the heaters is limited:

$$Q(\phi_i + \mathrm{d}\phi) = \begin{cases} -G_1\theta(\phi_i), & \theta(\phi_i) \leqslant 0 \\ 0, & \theta(\phi_i) > 0. \end{cases} \tag{4.2}$$

In order to find the optimal proportional gain $G_{1,opt}$ with which maximum suppression can be obtained, for each value of ϵ, a set of measurements with various G_1 was performed. G_1 was increased in steps from 0 until it exceeds $G_{1,opt}$. Normally, in order to achieve efficient increments of G to reach $G_{1,opt}$, the increments were set differently for different ϵ. Therefore, when drawing the bifurcation curves for constant values of G_1 as shown later, the data needed to linearly interpolated to compute the amplitudes in between the measured points. Between the measurements with different G_1, we let the system rest for a while so that the oscillation reverted back to the original state. Figure 8 shows how the amplitude of oscillation varies for different G_1 for three values of ϵ. As the gain is increased from zero, the root means square of the oscillation $(\overline{\theta(\phi_1)^2} + \overline{\theta(\phi_2)^2})^{1/2}$ is suppressed. The scheme starts to lose control as G_1 exceeds $G_{1,opt}$.

4.2. *Small* ϵ

When ϵ is small, the control shows an excellent performance with complete suppression of the oscillation achieved. Figure 9 shows the time history of the dimensionless temperature signal from one of the sensors, $\theta(\phi = 0)$, and corresponding power output, $Q(\phi = \pi)$. Here, $\epsilon = 0.18$ and $G_1 = G_{1,opt} = 2$. On turning on the control, the oscillation is damped completely within several periods. The system with the control loop shows a linear behaviour, where the exponential decay of the oscillation indicates that only the unstable mode is stabilized while other modes are unaffected. The heater output initially overshoots but then drops down to less than 1 mW as the control becomes successful. The effect of the control can be confirmed by the spectrum analysis shown in figure 10. It can be observed that all the frequency components

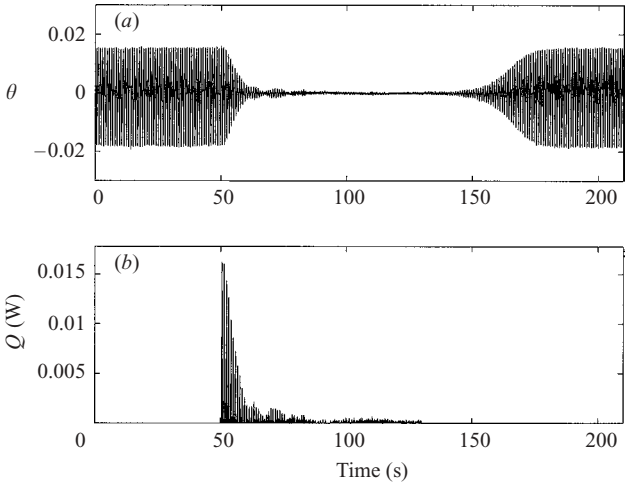

FIGURE 9. (*a*) Time history of the dimensionless temperature signal $\theta(\phi = 0)$. (*b*) Simultaneously measured heater output power $Q(\phi = \pi)$. $\epsilon = 0.18$.

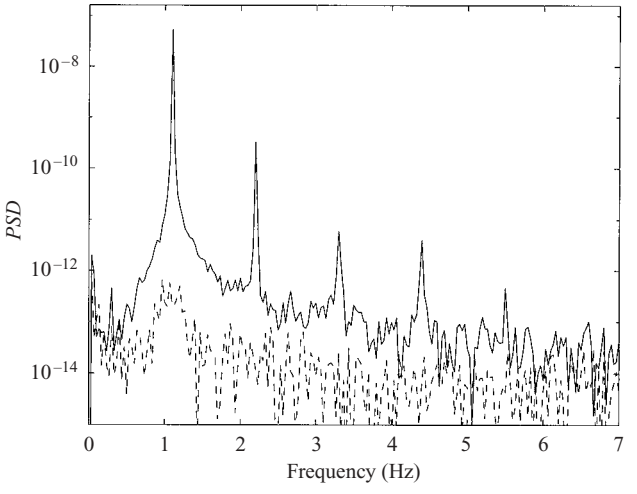

FIGURE 10. The power spectrum density of the non-dimensional temperature signal without control (solid line) and with control (dashed line) for $\epsilon = 0.18$.

have disappeared. Similar results can be obtained for the other sensor/heater pair; thus global stabilization of the oscillation is achieved.

The mean value of the temperature was recorded simultaneously, and no severe variation in the mean value was detected before, during, and after applying the control, which indicates that the heat delivered to the fluid during the control is sufficiently small to not alter the base state appreciably. This clearly shows that the mechanism for the stabilization of the oscillation flow is that the temperature fluctuation on the surface is counteracted without influencing the base flow. It can be seen from figure 9 that the magnitudes of the upper and lower bounds of the uncontrolled oscillations are slightly different. This is due to the harmonic waves superposed on the fundamental ones deforming the sinusoidal wave, and the mean value of θ is still 0.

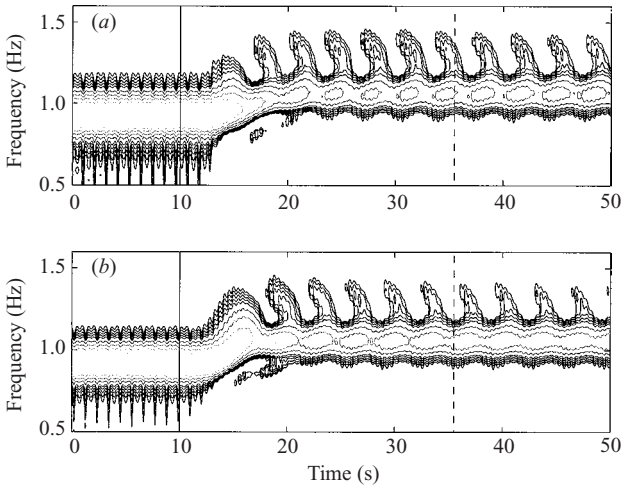

FIGURE 11. Wavelet analysis of the temperature signals $\theta(\phi_1, t)$ (a) and $\theta(\phi_2, t)$ (b) for $\epsilon = 0.52$.

One may wonder if the modification of local viscosity due to the heating plays a role in the mechanism. The variation in local surface temperature due to control heating should be of the same order as the amplitude of the initial temperature oscillation whose typical value is about 0.4 °C. The corresponding variation in viscosity of the liquid used in the present experiment is about 1%. As the amplitude of the suppressed oscillation is much smaller than the initial value, the viscosity variation should negligible and unlikely to play a role in the mechanism.

The successful global stabilization of the whole flow field can also be observed by flow visualization. On applying the control, the mode-2 standing wave with the elliptical particle-free area (figure 3*a–c*) gradually reaches a steady axisymmetric state, as shown in figure 3(*d*). Radial streaks appear in the particle-free area, which implies that the azimuthal velocity is absent.

4.3. *Larger* ϵ

On increasing ϵ further, the performance of the control deteriorates, even though non-trivial attenuation of the oscillation can still be observed. Figure 11 shows the wavelet transforms of the temperature signals, $\theta(\phi_1, t)$ (a) and $\theta(\phi_2, t)$ (b), for higher ϵ $(= 0.52)$. A Morlet wavelet was used (Goupillaud, Grossmann & Morlet 1984). The wavelet transforms allow us to observe the time evolution of the dominant frequency components. The contour lines indicate the energy of the disturbance. Turning on the control at $t = 10$ (solid line), the energy intensity gradually decreases as f_2 increases from 0.9 Hz to about 1.3 Hz at $t = 15$. When the control achieves a steady state, a modulation with a period of about 4 s appears on the f_2 components of both signals. As indicated by the vertical dashed lines, the two modulations are out of phase. This implies that the node of the oscillation is going back and forth between $\phi = 0$ and $\phi = \pi/4$ with a period of 4 s. This feature of the controlled standing wave was also observed by flow visualization, but not so clearly since the motion of mode-2 is overshadowed by the additional mode. At this stage, it is not clear whether this behavior is due to the nonlinear effect.

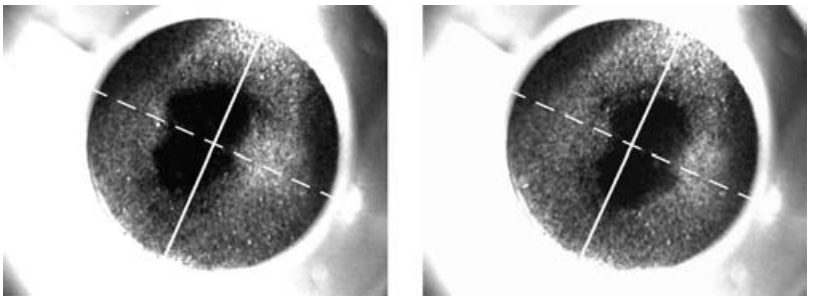

(*a*) $t = 0$ (*b*) $t = 0.48$ s

FIGURE 12. Flow visualization of excited mode-1 standing wave.

In addition, on turning on the control, a new frequency component appears which suggests the existence of a newly appearing mode. This was also observed by Shiomi & Amberg(2002) in the annular geometry when ϵ exceeds a certain value. The peak of the additional mode is about 1.05 Hz. On increasing G_1 further, the new mode becomes dominant over the original one.

4.4. *The appearance of mode* 1

The modification of the mode structure caused by the linear control, which limits the performance of the method (solid lines in figure 8), can be clarified by flow visualization. As can be seen in figure 12, on turning on the control, mode-2 oscillation becomes a mode-1 dominating standing wave. Here, the number of lines of symmetry is 1 as indicated by the line of symmetry (dashed lines). The solid lines denote the node lines of the oscillation. Following the sequence of pictures $(a) \leftrightarrow (b)$, it can be observed that most of the dark area moves to the other side of the node line. Note that the two pictures are mirror images of each other with respect to the node line. For the range of ϵ presented in this paper, the new mode-1 oscillation always has a standing structure. It is likely that when G_1 is above a certain value, bifurcation of mode-1 is encouraged, since the current control method causes amplification of waves with azimuthal wavenumber of 1. For a mode-1 oscillation, the temperature signals are out of phase for a sensor/heater pair when $\mathrm{d}\phi = \pi$, hence the oscillation will be amplified by a negative gain. Here, since there are two sensor/heater pairs $\pi/4$ apart from each other, the steady state is achieved when the anti-nodes of the oscillation are placed at the mid-points of the two sensors ($\phi = \pi/8$) and the two heaters ($\phi = 9\pi/8$).

The bifurcation curve of mode-1 is shown in figure 13. The amplitudes of the mode-1 oscillation for three different values of G_1 are shown with solid lines. The range of available data is not sufficient to make a conclusive statement on whether the bifurcation is supercritical or subcritical. For $G_1 = 10$ and 15, the bifurcation curve for smaller ϵ could not be drawn due to the limits of the tested range of parameter sets. For $G_1 = 5$, the bifurcation curve for larger ϵ is missing because A_1 could not be identified when mode-2 is dominant, and the bands of f_1 and f_2 overlap. Nevertheless, it can be observed that this is not the case where the control influences only the linear property of the system and the Hopf bifurcation is simply shifted downwards. The control does alter the nonlinear property, which results in a dramatic increase of the amplitude with increasing G_1.

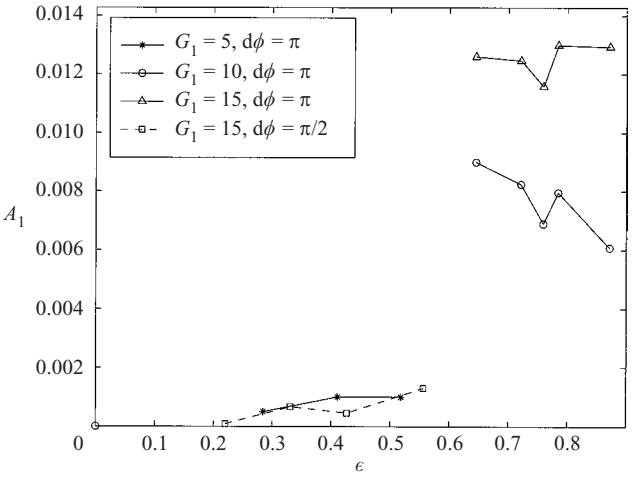

FIGURE 13. Mode-1 bifurcation for various G_1. Solid lines: $d\phi = \pi$, dashed line: $d\phi = \pi/2$. $A_1 = (A_{1,1}^2 + A_{1,2}^2)^{1/2}$. For $d\phi = \pi/2$, mode-1 oscillation is not observed for $G_1 = 5$ or 10.

5. Proportional control, $d\phi = \pi/2$

5.1. *Modified linear control*

One possible way to discourage the amplification of mode-1 is to change the azimuthal distance between the sensors and the heaters ($d\phi$). When $d\phi = \pi$, assuming the newly appearing mode-1 to be a standing wave, the mode will oscillate with its anti-nodes close to the sensors and heaters. Then we move the heater so that the scheme becomes

$$Q(\phi_i + \pi/2) = \begin{cases} G_1\theta(\phi_i), & \theta(\phi_i) \geqslant 0 \\ 0, & \theta(\phi_i) < 0. \end{cases} \tag{5.1}$$

With this change, instead of cancelling the temperature at a local position whose temperature is in phase with that at the sensor position, we carry out the cancellation at a local position whose temperature is out of phase with the sensor signal. Note that, in this case, the sign in front of G_1 needs to be changed to positive. In this way, as long as the mode-1 oscillation is standing, the amplification of mode-1 should be attenuated.

In the present experiment, for technical simplicity, the sensors and heaters were positioned as shown in figure 7(*b*), where sensors were positioned at $\phi_1 = 0$ and $\phi_2 = \pi/4$, and corresponding heaters were placed at $\phi = \phi_1 - \pi/2$ and $\phi = \phi_2 + \pi/2$, respectively.

Consequently, the changes in sensor/heater positioning resulted in a significant delay in the appearance of mode-1 compared with the case $d\phi = \pi$. As can be seen in figure 8, further increase of G_1 is allowed without triggering mode-1. The considerable delay in the mode-1 bifurcation can also be confirmed in figure 13, where mode-1 (solid lines) does not appear until G_1 reaches 15, even with small amplitude. Now complete suppression can be achieved up to $\epsilon = 0.41$ where the initial oscillation has a travelling structure. Mode transition does take place when G_1 is increased further, though, as shown later, the control suppresses the oscillation to less than 30% of the uncontrolled value in this range of ϵ before the transition takes place.

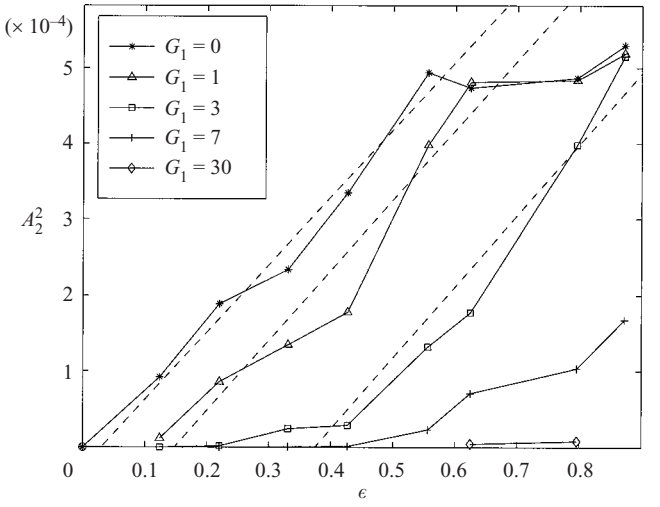

FIGURE 14. Mode-2 bifurcation for various G_1. Dashed lines represent the linear least-squares fit to the data.

5.2. *Mode-2 bifurcation*

The influence of the control in the context of bifurcation analysis is shown in figure 14. The dashed lines denote the bifurcation curve fit to the data obtained. The experimental results show a clear linear influence where the bifurcation curve is shifted along the horizontal axis as G_1 increases. Qualitatively similar results were obtained for $\mathrm{d}\phi = \pi$ when the mode-2 component was filtered through. On increasing G_1 to 30, the bifurcation curve falls on the horizontal axis, which means that the mode-2 oscillation is completely suppressed. For this value of G_1, however, mode-1 is amplified as can be seen in figure 13.

5.3. *Frequency*

As seen in figure 11, when applying the proportional control, the critical frequency of mode-2 (f_2) increases by a non-trivial amount. On increasing G_1 from 0, f_2 increases until $G_1 = G_{1,opt}$, above which the frequency saturates. The increase in f_2 can be explained by the fact, based on flow visualization and the computed oscillation amplitudes, that the flow pattern becomes more standing-wave-like as G_1 is increased and the amplitude of the oscillation is reduced. The structure of the oscillation becomes more similar to that at onset as the system is stabilized. The frequency saturates when the oscillation becomes a pure standing wave. In figure 6, values of f_2 for $G_1 = G_{1,opt}$ are depicted as circles for a range of ϵ. The solid line shows the linear increase of f_2 with control. It can be observed that the line matches f_2^{SW} well.

5.4. *Overall performance of the proportional control*

The overall performance of the proportional control is illustrated in figure 15. The performance of the control is quantified by the suppression ratio $\gamma(G_{1,opt})$, where γ is the ratio of θ_{rms} with control to θ_{rms} without control. Significant attenuation of the oscillation was obtained in the range of $\epsilon\ (\leqslant 0.9)$ presented. The optimal $\mathrm{d}\phi$ was $\pi/2$ in this range. The control showed an excellent performance when $\epsilon \leqslant 0.41$ where the

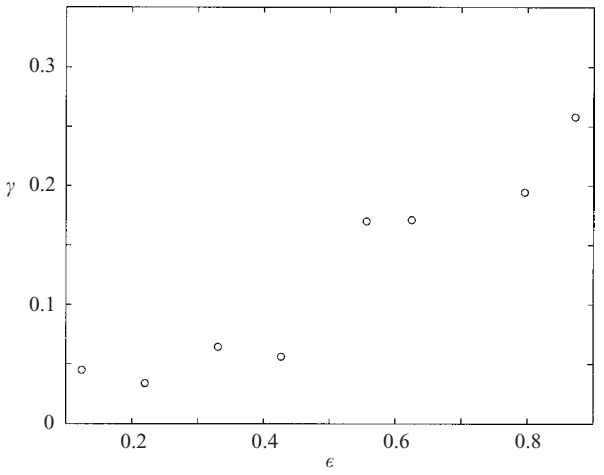

FIGURE 15. Performance of the proportional control over a range of ϵ. Circles: suppression ratio γ with optimal gain $G_{1,opt}$.

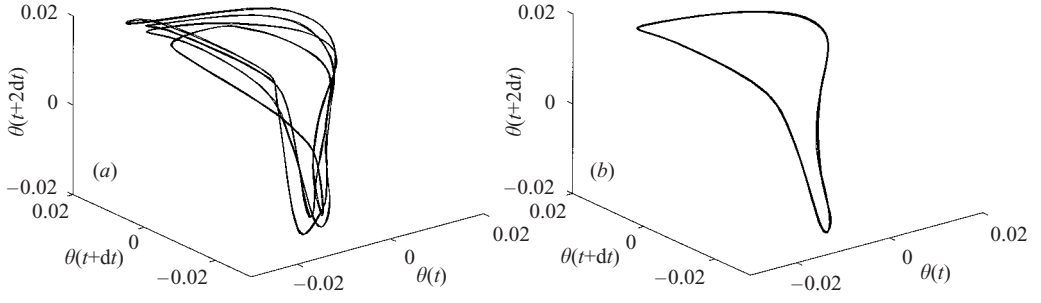

FIGURE 16. Three-dimensional return maps of the oscillation $\theta(\phi_1)$ in the period-doubling regime for (*a*) $G_1 = 0$ and (*b*) $G_1 = 5.4$. $\mathrm{d}\phi = \pi/2$, $\epsilon = 1.5$, $\mathrm{d}t = 0.16$ s.

oscillation was suppressed down to the level of background noise. This upper limit of ϵ is substantially larger then the value $\epsilon = 0.08$ reported by Petrov *et al.* (1998). Above that point $\gamma(G_{opt})$ increases gradually up to 0.26 as ϵ approaches 0.9.

5.5. *Proportional control in the period-doubling regime*

The proportional control with $\mathrm{d}\phi = \pi/2$ seems to work quite well even in the strongly nonlinear regime. To investigate how the control performs on a flow with even stronger nonlinearity and more chaotic characteristics, we have applied the proportional control to the oscillation with $\epsilon = 1.5$. Figure 16 (*a*, *b*) depicts the three-dimensional return map constructed from experimental time series of dimensionless temperature for different values of G_1. The delay is set to 0.16 s. Map (*a*) shows that the oscillation is in a state of period doubling with period-4 cycle, the beginning of a cascade which leads the system to chaos (May 1976). On applying the proportional control, as shown in the map (*b*), the control stabilizes the orbit, which becomes periodic. Similar stabilization was also observed from the other sensor. We could attenuate the amplitude of the oscillation by increasing G_1 even more. However, the maximum

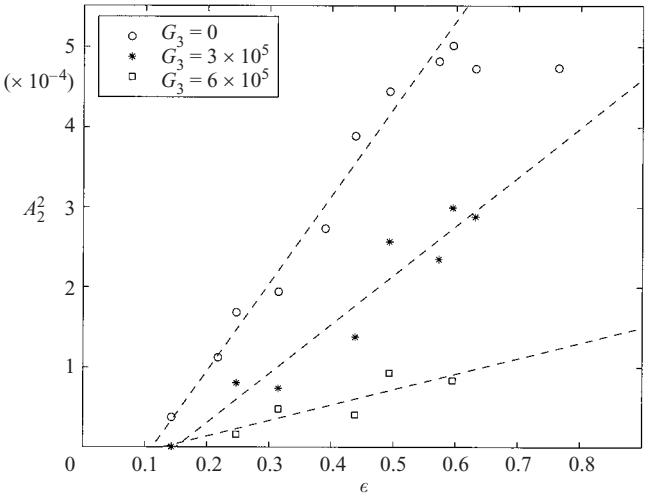

FIGURE 17. Influence of the cubic control on the bifurcation features of mode-2 for $d\phi = \pi$ and $G_1 = 0.8$.

power output limit of the heater prevented us from exploring the control with optimal G_1.

6. Cubic control

The cubic term was added to the control law as

$$Q(\phi_i + d\phi) = \begin{cases} -G_1\theta(\phi_i) - G_3\theta(\phi_i)(\theta(\phi_1)^2 + \theta(\phi_2)^2), & \theta(\phi_i) \leqslant 0 \\ 0, & \theta(\phi_i) > 0. \end{cases} \tag{6.1}$$

Cubic control is often applied to change the characteristics of bifurcation. Specifically, if the system shows a subcritical bifurcation, modification of the nonlinear properties of the system may render it supercritical which is more easily controlled (Yuen & Bau 1996). Observing the influence of the linear control scheme on the nonlinear property of mode-1, our original motivation to add the cubic term in the control law was to stabilize the higher-order terms of mode-1. To this end, we would need G_3 to be negative. Unfortunately, this may be problematic since it will amplify mode-2 and change its bifurcation from supercritical to subcritical.

However, there could still be benefits from applying cubic control with positive G_3. Figure 17 depicts the change in bifurcation curve with increasing G_3 and constant $G_1 (= 0.8)$. As would be expected, the cubic control decreases the slope of the bifurcation curve but does not affect the onset. Here $d\phi = \pi$, hence the mode transition should take place earlier than for $d\phi = \pi/2$. However, in the range of data presented, the bifurcation of mode-1 could not be observed although significantly more suppression is obtained compared to the case with only proportional control. This is understandable since the cubic control has a small influence on the linear properties of the system, hence it does not shift the onset of mode-1 bifurcation. Still, the limited influence on the linear properties does trigger mode-1 when G_3 exceeds a certain value beyond the range presented in figure 17. The cubic control also destabilizes the cubic properties of the mode-1 oscillation. It has been observed that, once mode-1 is triggered by increasing G_1, the onset amplitude of mode-1 is considerably increased as G_3 increases.

7. Conclusions

We have performed linear control on oscillatory thermocapillary convection in a half-zone. Configurations with different distances between two sensor/heater pairs were examined. When $d\phi = \pi$, the control was found to amplify mode-1 oscillation. This could be remedied by modifying the probe configuration so that the amplification is minimized. The proportional control shows an excellent performance in the weakly nonlinear regime. Up to $\epsilon = 0.42$, complete suppression of oscillations could be achieved. The linear scheme gradually loses control as the nonlinearity becomes stronger. However it should be noted that the linear control scheme achieves a significant attenuation up to fairly high ϵ. At least up to $\epsilon \sim 0.9$, the control suppresses the oscillation down to less than 30% of the initial value.

It should be pointed out that the control method with $d\phi = \pi/2$ is not able to directly suppress the harmonic modes since they are in phase at paired sensors and heaters, whereas the scheme is capable of suppressing the harmonics when $d\phi = \pi$ as long as the temperature signals at two locations $\pi/4$ apart are in phase. For $d\phi = \pi/2$, there is a risk that the harmonics are actually amplified. In spite of this difference, the two control methods seem to act on the mode-2 oscillation in quantitatively the same manner for the range of ϵ presented. This suggests that, even with a considerable amount of energy in harmonic modes, the performance of control relies mainly on suppressing the fundamental mode.

At high ϵ ($= 1.5$), where the period-4 cycle is observed, the control stabilizes the flow to a periodic state. Unfortunately, the present experimental setup did not allow us to raise ϵ to the chaotic regime without overheating the bridge supports. Since it is known that a chaotic state for high Pr can easily be achieved for example in an experiment performed in a freezer (Ueno *et al.* 2003), this should be possible in the near future.

It was also shown that cubic control can alter the nonlinear properties of the system in a beneficial way. Since the cubic term has little effect on the linear properties, it does not promote the bifurcation of mode-1 as much as the linear control does. Choosing the right combination of G_1 and G_3, it should be possible to achieve the best suppression of the mode-2 oscillation before triggering mode-1.

The stay of J. Shiomi in Japan was supported by the Sweden Japan Foundation. This work was partially supported by the Swedish Research Council (VR).

REFERENCES

Bau, H. H. 1999 Control of Marangoni-Bénard convection. *Intl J. Heat Mass Transfer* **42**, 1327–1341.

Benz, S., Hinz, P., Riley, R. J. & Neitzel, G. P. 1998 Instability of thermocapillary–buoyancy convection in shallow layers. Part 2. Suppression of hydrothermal waves. *J. Fluid Mech.* **359**, 165–180.

Chang, C. E. & Wilcox, W. R. 1976 Analysis of surface tension driven flow in floating zone melting. *Intl J. Heat Mass Transfer* **19**, 355–356.

Chun, C. H. & Wuest, W. 1979 Experiments on the transition from the steady to the oscillatory Marangoni-convection of a floating zone under reduced gravity effect. *Acta Astron.* **6**, 1073–1082.

Goupillaud, P., Grossmann, A. & Morlet, J. 1984 Cycle-octave and related transforms in seismic signal analysis. *Geoexploration* **23**, 85–102.

Howle, L. E. 1997 Control of Rayliegh-Bénard convection in a small aspect ratio container. *Intl J. Heat Mass Transfer* **40**, 817–822.

Hu, W. R., Shu, J. Z., Zhou, R. & Tang, Z. M. 1994 Influence of liquid bridge volume on the onset of oscillation in floating zone convection. *J. Cryst. Growth* **142**, 379–384.

Iooss, G. & Joseph, D. D. 1989 *Elementary Stability and Bifurcation Theory*, 2nd edn. Springer.

Kawamura, H., Ueno, I. & Ishikawa, T. 2002 Study of thermocapillary flow in a liquid bridge towards an on-orbit experiment aboard the International Space Station. *Adv. Space Res.* **29**, 611–618.

Kuhlmann, H. C. & Rath, H. J. 1993 Hydrodynamic instabilities in cylindrical thermocapillary liquid bridges. *J. Fluid Mech.* **247**, 247–274.

Levenstam, M. & Amberg, G. 1995 Hydrodynamical instabilities of thermocapillary flow in a half-zone. *J. Fluid Mech.* **297**, 357–372.

Levenstam, M., Amberg, G. & Winkler, C. 2001 Instabilities of thermocapillary convection in a half-zone at intermediate Prandtl numbers. *Phys. Fluids* **13**, 807–816.

Leypoldt, J., Kuhlmann, H. C. & Rath, H. J. 2000 Three-dimensional numerical simulation of thermocapillary flows of cylindrical liquid bridges. *J. Fluid Mech.* **414**, 285–314.

May, R. M. 1976 Simple mathematical models with very complicated dynamics. *Nature* **261**, 459–467.

Neitzel, G. P., Chang, K. T., Jankowski, D. F. & Mittelmann, H. D. 1993 Linear stability theory of thermocapillary convection in a model of the float-zone crystal-growth process. *Phys. Fluids* A **5**, 108–114.

Or, A. C. & Kelly, R. E. 2001 Feedback control of weakly nonlinear Rayleigh-Bénard-Marangoni convection. *J. Fluid Mech.* **440**, 27–47.

Or, A. C., Kelly, R. E., Cortelezzi, L. & Speyer, J. L. 1999 Control of long-wavelength Marangoni-Bénard convection. *J. Fluid Mech.* **387**, 321–341.

Ott, E., Grebogi, C. & Yorke, J. A. 1990 Controlling chaos. *Phys. Rev. Lett.* **64**, 1196–1199.

Petrov, V., Muehlner, K. A., VanHook, S. J. & Swinney, H. L. 1998 Model-independent nonlinear control algorithm with application to a liquid bridge experiment. *Phys. Rev.* E **58**, 427–433.

Petrov, V., Schatz, M. F., Muehlner, K. A., VanHook, S. J., McCormick, W. D., Swift, J. B. & Swinney, H. L. 1996 Nonlinear control of remote unstable states in a liquid bridge convection experiment. *Phys. Rev. Lett.* **77**, 3779–3782.

Preisser, F., Schwabe, D. & Scharmann, A. 1983 Steady and oscillatory thermocapillary convection in liquid columns with free cylindrical surface. *J. Fluid Mech.* **126**, 545–567.

Schwabe, D., Hintz, P. & Frank, S. 1996 New features of thermocapillary convection in floating zones revealed by tracer particles accumulation structures (PAS). *Microgravity Sci. Technol.* **9**, 163–168.

Schwabe, D. & Scharmann, A. 1979 Some evidence for the existence and magnitude of a critical Marangoni number for the onset of oscillatory flow in crystal growth melts. *J. Cryst. Growth* **6**, 125–131.

Shiomi, J. & Amberg, G. 2002 Active control of a global thermocapillary instability. *Phys. Fluids* **14**, 3039–3045.

Shiomi, J., Amberg, G. & Alfredsson, P. H. 2001 Active control of oscillatory thermocapillary convection. *Phys. Rev.* E **64**, 031205.

Tang, J. & Bau, H. H. 1993 Feedback control stabilization of the no-motion state of a fluid confined in a horizontal, porous layer heated from below. *J. Fluid Mech.* **257**, 485–505.

Tang, J. & Bau, H. H. 1998 Experiments on the stabilization of the no-motion state of a fluid layer heated from below and cooled from above. *J. Fluid Mech.* **363**, 153–171.

Ueno, I., Tanaka, S. & Kawamura, H. 2003 Oscillatory and chaotic thermocapillary convection in a half-zone liquid bridge. *Phys. Fluids* **15**, 408–416.

Velten, R., Schwabe, D. & Scharmann, A. 1991 The periodic instability of thermocapillary convection in cylindrical liquid bridges. *Phys. Fluids* A **3**, 267–279.

Wang, Y., Singer, J. & Bau, H. H. 1992 Controlling chaos in a thermal convection loop. *J. Fluid Mech.* **237**, 479–498.

Wanschura, M., Shevtsova, V. M., Kuhlmann, H. C. & Rath, H. J. 1995 Convective instability mechanisms in thermocapillary liquid bridges. *Phys. Fluids* **7**, 912–925.

Yuen, P. K. & Bau, H. H. 1996 Rendering a subcritical Hopf bifurcation supercritical. *J. Fluid Mech.* **317**, 91–109.